ELSEVIER

Contents lists available at ScienceDirect

Journal of Colloid and Interface Science

journal homepage: www.elsevier.com/locate/jcis



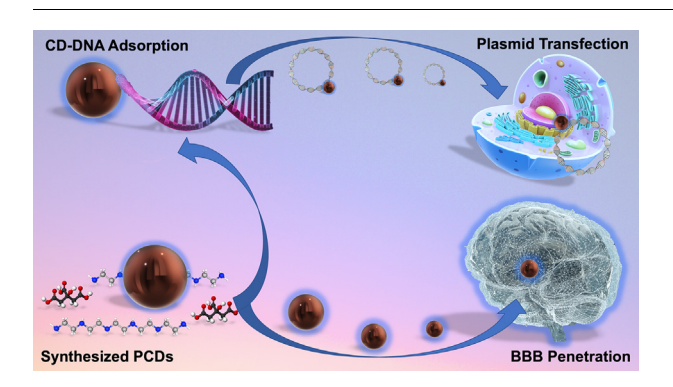
Nano-carrier for gene delivery and bioimaging based on pentaetheylenehexamine modified carbon dots



Wei Zhang ^{a,1}, Jiuyan Chen ^{a,1}, Jun Gu ^a, Mattia Bartoli ^b, Justin B. Domena ^a, Yiqun Zhou ^{a,c}, Braulio C.L.B. Ferreira ^a, Emel Kirbas Cilingir ^a, Caitlin M. McGee ^a, Rachel Sampson ^c, Chiara Arduino ^{a,c}, Alberto Tagliaferro ^b, Roger M. Leblanc ^{a,*}

- ^a Department of Chemistry, University of Miami, Coral Gables, FL 33146, USA
- ^b Department of Applied Science and Technology, Politecnico di Torino, Italy

G R A P H I C A L A B S T R A C T



ARTICLE INFO

Article history:
Received 22 December 2022
Revised 10 February 2023
Accepted 11 February 2023
Available online 15 February 2023

Keywords: Carbon dots Pentaethylenehexamine Cellular uptake Blood-brain barrier penetration Nucleic acid/gene delivery

ABSTRACT

Carbon dots (CDs) have attracted much attention due to their excellent properties and applications, especially the use for gene delivery. Considering the risks and concerns involved in the use of viral vectors for gene delivery in vivo, non-viral vectors such as CDs have gradually become an ideal alternative due to their biocompatibility and low toxicity. Therefore, in this study, the potential to apply CDs as a nonviral vector for gene delivery was investigated. The CDs were prepared using citric acid and pentaethylenehexamine (PEHA) as precursors via a one-step microwave-mediated approach. The optical, structural, and morphological properties of PEHA-derived CDs (PCDs) were characterized by ultraviolet spectroscopy (UV-vis), photoluminescence (PL), Fourier Transform Infrared spectroscopy (FTIR), thermogravimetric analysis (TGA), X-ray photoelectron spectroscopy (XPS), zeta potential, circular dichroism spectrometry, atomic force (AFM) and transmission electron microscopies (TEM). The analysis demonstrated that the as-prepared PCDs were rich in amine groups and were positively charged. Subsequently, gel retardation assay showed that PCDs could non-covalently bind with DNA at a mass ratio of 2:1 (PCDs: DNA). Additionally, PCDs possessed a tremendously lower cytotoxicity compared with polyethylenimine (PEI), a popular precursor/dopant for many CDs preparations, and their plasmid composite showed a high transfection efficiency. Meanwhile, PCDs were also observed to cross the bloodbrain barrier (BBB) by using a zebrafish model. In conclusion, these results significantly indicate that

E-mail address: rml@miami.edu (R.M. Leblanc).

^c C-Dots, LLC, Miami, FL 33136, USA

^{*} Corresponding author.

¹ These authors contribute equally to this work.

PCDs are a potential non-viral nucleic acid/gene vector to gene therapy. Also, PCDs can be utilized in drug delivery for treating brain diseases, such as Alzheimer's disease and brain tumors.

© 2023 Elsevier Inc. All rights reserved.

1. Introduction

The 21st century is witnessing a prosperous development of genetic engineering which is increasingly applied to modern medicine by modifying and manipulating organism's genes using nanotechnology [1,2]. Gene delivery is an essential step in gene therapy by introducing foreign genetic materials into host cells to integrate into their genome or replicate and express themselves independently [3,4]. To keep the delivered genes stable, a common practice is to conjugate the genes to a genetic vector which can also promote the efficiency of gene delivery and facilitate the manipulation of genes in the host cells [5,6]. The genetic vectors are mainly categorized into viral vectors and non-viral vectors. Gene delivery using viral vectors takes the advantages of the ability of viruses to inject intended genetic materials into the host cells while being non-infectious [6]. However, there are also challenges for using viral vectors, such as viral vectors can potentially induce immune responses, only small pieces of genetic materials can be delivered, and there are risks of random insertion sites, cytopathic effects, and mutagenesis [7]. In comparison, non-viral vectors do not induce significant immune responses, can deliver larger genetic materials, and are more reproducible which makes it attract more attention in recent years [8,9].

Non-viral vectors can be grouped as carrier-free vectors and carrier-based vectors [10]. The carrier-free vectors facilitate the delivery of genetic materials into cells by using physical methods, including electroporation, particle bombardment, sonoporation, photoporation, magnetofection that utilize electrical pulses, force, sound, light, and magnetic fields to increase the permeability of cell membranes to allow genetic materials entering cells [11–16]. However, these physical methods often cause a high rate of cell death during the process [17]. Carrier-based vectors employ synthetic or natural biocompatible materials as carriers to deliver genetic materials [18,19]. The commonly used carrier-based vectors, such as liposomes, inorganic nanoparticles (NPs), and polymeric NPs, can bind to genetic materials electrostatically and enter cells by endocytosis to deliver genetic payloads [18-21]. The carrier-based vectors can encapsulate genetic materials to protect them from degradation during the delivery process [10]. Despite their advantages, non-viral vectors haven't been used much due to their relatively low efficiency of gene delivery [22]. There is an urgent need to develop new nanomaterials to overcome this limitation of non-viral vectors [23,24].

Carbon dots (CDs) are a unique type of carbon-based nanoparticles less than 10 nm in size and a promising kind of drug nanocarrier which can penetrate cell membranes via mechanisms like phagocytosis, endocytosis, and micropinocytosis [25-27]. Other properties of CDs including low cytotoxicity, good biocompatibility, water solubility and photoluminescence (PL) make them a versatile drug nanocarrier and can be tracked in real-time in the cells [28]. CDs possess abundant surface functional groups which can be easily functionalized with inorganic and organic molecules [29]. It has been reported that CDs with abundant amine groups resulting in positive charges on the surface can bind to the negatively charged DNA or RNA by electrostatic interaction to form CDs-DNA/RNA complexes and deliver the attached DNA or RNA into cells [21,30–32]. To further improve the binding efficiency, more positively-charged CDs are needed which can be achieved by using positively charged molecules as the precursors, like polyethyleneimine (PEI), polyethylene diamine (PAMAM), chitosan, poly-L-lysin (PLL), and pentaethylenehexamine (PEHA) for the synthesis of CDs [33]. Among them, PEHA containing four secondary amine groups and two primary amine groups has been used to synthesize positively charged CDs [34]. However, there are limited reports about using PEHA-synthesized CDs to deliver genetic materials into cells and to cross the blood–brain barriers (BBB).

Herein, in this study, a new type of CDs, namely PCDs, were synthesized using citric acid and PEHA as precursors. Various physicochemical properties of PCDs were studied by UV/vis absorption, PL, Fourier-transform infrared (FTIR) spectroscopies, X-ray photoelectron spectroscopy (XPS), atomic force microscopy (AFM), transmission electron microscopy (TEM), thermogravimetric analysis (TGA), derivative thermogravimetry (DTG), circular dichroism spectrometry and zeta potential measurements. In order to assess the binding efficiency of PCDs and DNA, agarose gel retardation assay was conducted at different mass ratios between PCDs and DNA. In addition, UV/vis absorption, fluorescence emission, and circular dichroism spectroscopies were applied to elucidate the binding mechanisms. Subsequently, PCDs composited with plasmid were followed by cell viability and transfection capacity studies in comparison to PEI which is a commercial transfection reagent. In the end, zebrafish was applied as an in vivo model to explore the possibility of PCDs to penetrate the BBB by closely monitoring central canal of spinal cord following the intravascular injection of PCDs.

2. Experimental section

2.1. Materials

PEHA (\geqslant 98 %), citric acid (\geqslant 98 %), MTT (CAT# M2128) and mouse anti-β-actin (CAT# A5441) were ordered from Sigma-Aldrich (St. Louis, MO, USA). The dialysis tubing with a MWCO of 100–500 Da was obtained from Spectrum Labs, Inc. (Rancho Dominguez, CA). Deionized (DI) water (resistivity: 18.2 MΩ.cm; surface tension: 72.6 mN·m⁻¹; pH: 6.6 ± 0.3 at 20.0 ± 0.5 °C) was acquired using a MilliQ3 water purification system obtained from Millipore Sigma (Burlington, MA) and used as the solvent in the preparation of CDs. GFP and mCherry plasmids were bought from VectorBuilder (Santa Clara, CA, USA). Mouse anti-GFP antibody (CAT# SC-9996) and anti-mouse IgG secondary antibodies (CAT# 926–32210 and 102673–408) were purchased from Santa Cruz (Dallas, TX, USA) and LI-COR (Lincoln, NE, USA), respectively. All the chemicals were used without further treatment.

2.2. Preparation of carbon dots

500 mg of citric acid and 0.5 mL PEHA were dissolved in 20 mL DI water and vigorously stirred overnight. Then, the mixed solution was heated in a domestic microwave oven at 700 W for 7 min. The resulting brown solid product was re-dispersed in 15 mL DI water, sonicated at 42 kHz for 90 min and centrifuged twice (9000 rpm/30 min/4 °C). The supernatant was filtered (0.2 μm filter pore size) and dialyzed (MWCO: 100–500 Da) against DI water for 3 days (water was replaced every 24 h). The powder of PEHA-derived CDs was named as PCDs.

2.3. Characterization

UV/vis spectrophotometer (Agilent Cary 100) was used to acquire UV/vis absorption spectra. PL characterizations were carried out with a HORIBA Jobin Yvon Fluorolog-3 fluorometer with a slit width of 5 nm for both excitation and emission. Normalizations of PL emission spectra were achieved by using OriginPro 9.1 software. Quartz cuvettes with an optical pathlength of 1 cm were used for all the optical property characterizations. The attenuated total reflection FTIR (ATR-FTIR) spectroscopy was conducted on a FTIR spectrometer (FT-Nicolet 5700, Thermo Scientific) equipped with a Smartorbit (Thermo Scientific) operation. The AFM data were obtained with a 5420 atomic force microscope (Agilent Technologies) by placing a drop of PCDs aqueous solution (0.1 mg/mL) on a clean silica mica slide, followed by screening in tapping mode with an applied force of 3 N/m. TEM with a JOEL $1200 \times \text{was}$ applied to confirm the particle size of PCDs. TGA was conducted using a Netzsch TG 209 F3 Tarsus thermomicrobalance (Netzsch, USA) by heating the sample from 40 to 1000 °C at a rate of 10 °C/min under the protection of nitrogen gas. The zeta potential of PCDs was measured in a DLS nano series Malvern Zetasizer (Westborough, MA). The XPS spectra were recorded by using a PHI 5000 Versaprobe (Physical Electronics, Chanhassen, MN) scanning X-ray photoelectron spectrometer equipped with a monochromatic Al K-alpha X-ray source (1486.6 eV energy, 15 kV voltage, and 1 mA anode current). The circular dichroism analyses were conducted using an JASCO J-810 spectropolarimeter under than range of 200-340 nm, the parameters (scanning speed: 200 nm/min, accumulation:4) were set up to obtain a reliable data. Each characterization study was repeated with three independent batches of PCDs to validate the reliability of the results.

2.4. Determination of fluorescence quantum yield

Quinine sulfate and harmane were selected as two reference standards because the quantum yield (QY) of quinine sulfate and harmane in literature are 54 and 83 %, respectively. To measure the fluorescence quantum yield (QY) of PCDs, first of all, quinine sulfate and harmane were dissolved in 0.1 M $\rm H_2SO_4$ (refractive index, $\rm n_R$ = 1.33) for preparations of reference standards. PCDs were dissolved in DI water (refractive index, $\rm n_R$ = 1.33). The UV/vis spectrum at 350 nm of both standards and PCDs were controlled under an absorbance of 0.05. And the PL emission spectra of standards and PCDs were recorded with an excitation wavelength of 350 nm. Averages of absorbance and PL spectral integrated areas were inserted to the following equation:

$$\Phi = \Phi_R \times (I / I_R) \times (A_R / A) \times (n^2 / n_R^2).$$

In this equation, Φ represents the QY, I indicates the integrated area under the PL curve, A denotes the absorbance at 350 nm, n represents the refractive index. Subscript $_R$ is denoted for the reference standard.

2.5. Agarose gel retardation assay

Agarose gel electrophoresis was conducted to study PCDs binding with DNA. Briefly, 0.8, 8, 80, and 800 μ g/mL of PCDs aqueous solutions were prepared. Then, DNA-PCDs complexes at different mass ratios of PCDs to DNA (0.002:1, 0.02:1, 0.2:1 and 2:1) were prepared by separately adding 1 μ L of as prepared PCDs solutions (0.8, 8, 80, and 800 μ g/mL) to 9 μ L of 317, 734 and 1688 bp DNA solutions (400 μ g/mL). The as-obtained solutions were incubated at room temperature for 30 min, followed by agarose gel electrophoresis analysis in TAE buffer for 60 min at 120 V. The results were observed using BioRad-image lab software with UV light. The aforementioned DNA solutions were applied as controls.

DNA sequences information were as follows:

317 bp DNA primers: forward: TGTGCCTGCCAGAATC-CAAAGCCCT and reverse: CAGGGCCATGGTTTCCACAGCTACT.

734 bp DNA primers: forward: GACTCTGCTGTAA-GAAGGCCGGCA and reverse: CCCACAGTCTGAGCGCGGCCAATG.

1688 bp DNA primers: forward: TGGTGGTGTCAGTACGTTGG and reverse: AATGTGACAAACTAGCAGTCAACAA.

Each study was repeated three times to validate the reliability of the results.

2.6. MTT cell viability assay

HEK293 cells were cultured with high glucose in DMEM (with 10 % FBS and 1 % of penicillin–streptomycin) and seeded in 96-well tissue culture plates at a density of 5×10^3 cells/well. After culture for 24 h, cells were treated with PCDs, PEHA and PEI in a DMEM medium at different dose levels ranging from 0 to 62.5 $\mu g/mL$ for 72 h. Then, each well was added by 10 μL MTT (5 mg/mL) and incubated for 4 h. The formazan crystals were solubilized in acidic isopropanol after removal of the DMEM medium. The absorbance was measured by Tecan Microplate Readers at 595 nm. Results are shown as percentages of control group (0 $\mu g/mL$). Each study was repeated three times to validate the reliability of the results.

2.7. Carbon dot-mediated transfection

For the PCDs-mediated transfection, plasmids that express GFP (pDNA-GFP) and mCherry (pDNA-mCh) were used as reporter plasmids. HEK293 cells were seeded onto 35 mm glass-bottom dishes for 24 h and then transfected by plasmid-PCD complexes. Briefly, plasmid-PCDs complex solutions were prepared by mixing plasmid and PCDs at different mass ratios (1:20, 1:50 and 1:100; 1 μg of plasmid was applied to each well) in a DMEM medium at room temperature for 20 min. Then, the plasmid-PCDs complex solutions were added into wells and the cells were incubated for 4 h for transfection. Subsequently, the DMEM medium was discarded and a fresh DMEM medium was applied. After 48 h, the transfection efficiency was measured by detecting the GFP or mCherry signal via the use of a Zeiss fluorescence microscope. Each study was repeated three times to validate the reliability of the results.

2.8. Western blot

The cells transfected by GFP plasmid were collected after 48 h incubation. The cells were first washed with phosphate buffered saline (PBS) and lysed with RIPA buffer that contained proteinase and phosphatase inhibitor. The protein level was determined by BCA Protein Assay and 30 μ g of total protein was boiled with 1X Laemmli SDS-loading buffer for 5 min. The protein samples were separated on 10 % SDS-PAGE gel and transferred onto Nylon membrane. The membrane was blocked with Rockland Blocking Buffer for 1 hr and incubated with mouse anti-GFP antibody and mouse anti- β -actin at 4 °C overnight. The membrane was further incubated with an anti-mouse IgG secondary antibody for 1 hr at room temperature. The membrane was scanned using an Odyssey LI-COR device and images were analyzed by Image Studio Lite software. The results were expressed as the ratios to β -actin immunoreactivity and the final values were shown as the ratios to control group.

2.9. Zebrafish bioimaging

Wild-type zebrafish (*Danio rerio*) at 5 days post fertilization (dpf) were obtained from the University of Miami Zebrafish Core Facility. 100 nL of 50 mg/mL aqueous solution of PCDs was intravascularly injected into the heart of zebrafish larvae (number:

6) previously anesthetized by tricaine. Subsequently, the injected larvae were imaged using Leica SP5 confocal microscope under both white light and an excitation wavelength of 405 nm. The animal care protocol for all procedures used in this experiment was approved by the University of Miami Animal Care and Use Committee and complies with the guidelines of the National Science Foundation.

3. Results and discussion

3.1. Preparation and characterization of PCDs

PEHA and citric acid were used as precursors in this study. Water-soluble PCDs were synthesized using a microwaveassisted approach reported by our previous study [35]. The asprepared PCDs were purified via centrifugation, filtration, and dialysis to remove unreacted precursors and any intermediates formed during the synthesis of PCDs. The UV/vis spectrum (Fig. 1A) of PCDs shows a broad band at 350 nm that can be attributed to $n-\pi^*$ electronic transition of C=O and/or C=N structures [35,36]. The other absorption band of PCDs at 242 nm can be assigned to π - π * electronic transition of C=C [36]. PL is one of the most crucial properties of CDs in biomedical applications. The fluorescence emission spectra of PCDs in Fig. 1B show an excitation-dependent PL emission in the range of 400-600 nm with the maximum PL emission at 450 nm upon the excitation at 370 nm. In comparison, the fluorescence spectra of PEHA (Fig. S1) show the same maximum emission as PCDs at 450 nm but different maximum excitation at 350 nm. Moreover, to make sure the QY results are reliable and valid, appropriate reference standards, namely quinine sulfate and harmane, were applied for cross-calibration considering the similarity in PL behavior between them and PCDs. According to our previous studies,[37] the excitation wavelength of both standards and PCDs was set at 350 nm. Finally, by cross-calibration, the QY of quinine sulfate and harmane were calculated as 56.5 % (literature Φ = 54 %) and 80.6 % (literature Φ = 83 %), respectively. These results support the reliability of the assay. Subsequently, the same protocol was followed for the QY calculation of PCDs and a result of 2.1 % was calculated by standards used in the determination.

PCDs under day light (left) and 365-nm UV light irradiation (right). (B) Fluorescence emission spectra of PCDs in aqueous medium at a mass concentration of 1.25 \times 10^{-4} mg/mL. Inset are the normalized spectra.

In order to identify the functional groups of PCDs, FTIR spectroscopy was exploited. As shown in Fig. 2, citric acid as one of the two precursors provided carboxyl groups to PCDs. The spectrum of citric acid (Fig. 2A) shows three specfic patterns of peaks: the first peak pattern includes peaks at 3489, 3295 and 3195 cm⁻¹ that are attributed to O-H stretching; the second peak pattern such as 1754 and 1687 cm⁻¹ correspond to the C=O streching; the third peak pattern at around 1382 cm⁻¹ can be ascribed to the stretching vibration of C-O bonds [38]. The other peaks at 2751, 2657 and 2555 cm⁻¹ correspond to the C-H stretching and the peak at 1149 cm⁻¹ can be assigned to O—H bending [37]. Additionally, PEHA as the other precursor provided amine groups enabling PCDs to be positively charged. Fig. 2B shows peaks at 3356 and 3286 cm^{-1} that are attributed to N—H stretching. Peaks at 2903 and 2798 cm⁻¹ indicate the stretching vibration of C-H bonds. The peaks at 1592 and 1462 cm⁻¹ correspond to N—H and C-H bending, respectively. The two peaks at 1341 and 1272 cm⁻¹ can be assigned to C—N stretching [39]. In comparison, the FTIR spectrum of PCDs (Fig. 2C) shows a broad band at 3252 cm⁻¹, a characteristic IR peak indicating N—H and O—H stretching. Bands at 2933 and 2816 can be assigned to the C-H

stretching and 1436 cm⁻¹corresponding to the C—H bending. The other peaks at 1643, 1545, 1356, 1261and 1123 cm⁻¹ denote C=O stretching, N—H bending, C—O stretching, C—N stretching and O—H bending, respectively.

TGA was also conducted to investigate the thermal stability and structure of PCDs. According to our previous study, there were four stages of the mass loss of CNDs which represent the evaporation of water molecules (at 40-168 °C), the decomposition of oxygencontaining functional moieties (at 168–338 °C), the decomposition of amines to release ammonia gas (at 338-448 °C), and the decomposition of carbon nitride structures (at 448-1000 °C), respectively [40]. According to the TGA and DTG of PCDs (Fig. 3A and 3B), the 7.48 % mass loss at 40-103 °C resulted from the evaporation of water molecules adsorbed on the surface of PCDs. The second stage at 103-454 °C was due to the loss of "shell" of PCDs. In this stage, the water molecules formed through dehydration condensation reactions of alcoholic -OH was evaporated at 103-161 °C. The edge-plane oxygen-containing functional moieties (-COOH and/ or C=O) were decomposed at 161-339 and 339-381 °C while forming phenols and releasing CO and CO₂ respectively. The mass loss at 381–454 °C was ascribed to the decomposition of amines to release ammonia gas. The last stage at 454-1000 °C indicated the decomposition of the "core" of PCDs. After calcination at 1000 °C, there was nearly no remnant and the highest decomposition temperature almost reached 700 °C, which demonstrates an excellent chemical and thermal stabilities of PCDs. In addition, with the mass loss due to moisture excluded, the contents of "shell" and "core" of PCDs are 53.44 and 46.56 %, respectively.

To further study the structure of PCDs, XPS spectra and main XPS features of P-CDs were presented in Fig. 4 and summarized in Table S1, respectively. Table S1 displays the elemental composition of PCDs with oxygen and nitrogen occupying 18 and 13 %, respectively. It is worth noting that the content of nitrogen in PCDs is higher than many reported CDs,[37,41] which significantly contributes to the positive surface charge of PCDs. In contrast, carbon takes up 69 % and its functionalities include sp² hybridized carbon (284.6 eV, 56 %), C-X (X = 0, N, 285.6 eV, 31 %) and C = X (X = 0, N, 285.6 eV, 31 %)287.1 eV, 13 %). Interestingly, carboxylic functionalities were not detected neither in C1s nor in O1s spectra (Fig. 4A and 4B). O1s spectra clearly show a single peak with two well-defined components at 530.4 and 531.5 eV due to hydroxyl residues and carbonyl compounds, respectively. No peaks related to the carboxylic residues are present (535.0-535.3 eV). Nitrogen-containing species exhibit a massive presence of pyrrolic nitrogen (N5) and amino residues up to 72 % and comparable amounts of pyridinic nitrogen (N6) and graphitic nitrogen (NQ) of 14 and 13 %, respectively. The existence of C-O, C-N, C=O, O-H and N-H bonds are consistent with the FTIR analysis in Fig. 2C. Nonetheless, a small peak centered at 537.3 eV was observed suggesting the presence of N-O [42]. This was also supported by the presence of a small peak centered at 405.7 eV in the N1s spectra (Fig. 4C). Unfortunately, there is no obvious peak to show N-O bond in FTIR spectrum of PCDs. It is probably because N-O bonds only occupy 1 %-2% in Table S1, and there is a broad peak at around 1436 cm⁻¹ in Fig. 2C that may have overlapped with the peak denoting N-O bonds. Furthermore, the zeta potential of PCDs was + 6.73 mV (Fig. S2) that benefits their binding to the DNA or RNA through electrostatic interactions.

AFM and TEM images of PCDs were attained to understand the morphology and size distribution of PCDs (Fig. 5). To avoid self-aggregation of PCDs, a PCD aqueous solution was sonicated for 30 min prior to AFM and TEM screening. TEM allows for the most accurate estimation of the PCDs homogeneity on the x-y plane. AFM measures the particle sizes along the z-axis. In this study, PCDs present a narrow size distribution with a mean height of 2 nm from AFM. TEM images exhibit a wider and asymmetric gaus-

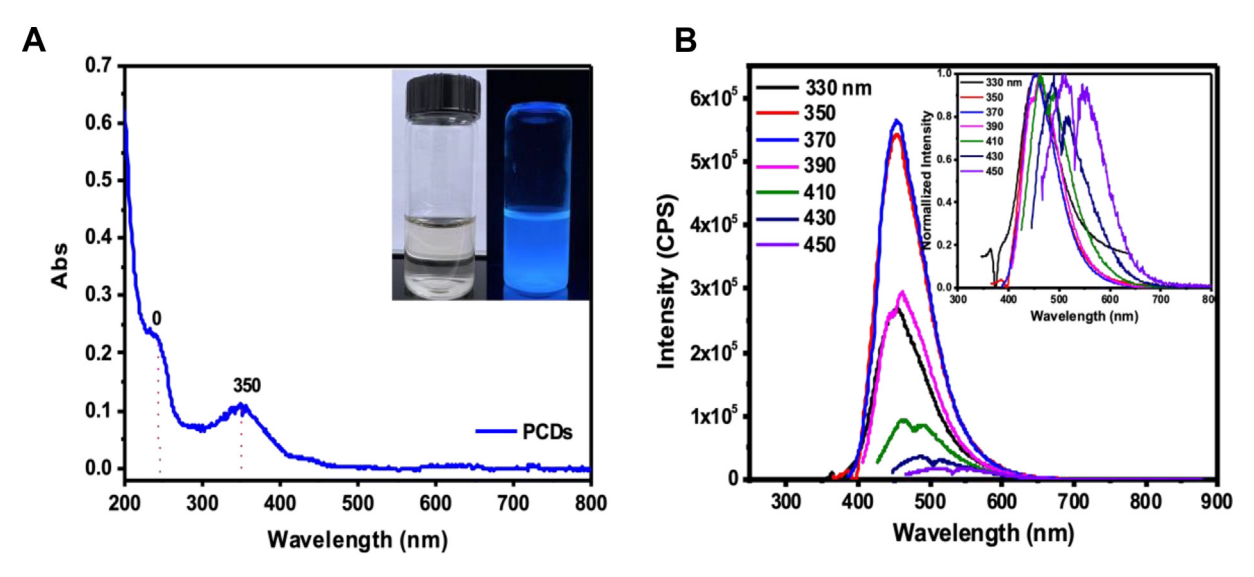


Fig. 1. (A) UV/vis absorption spectrum of a PCD aqueous solution (0.02 mg/mL). Inset are water-soluble.

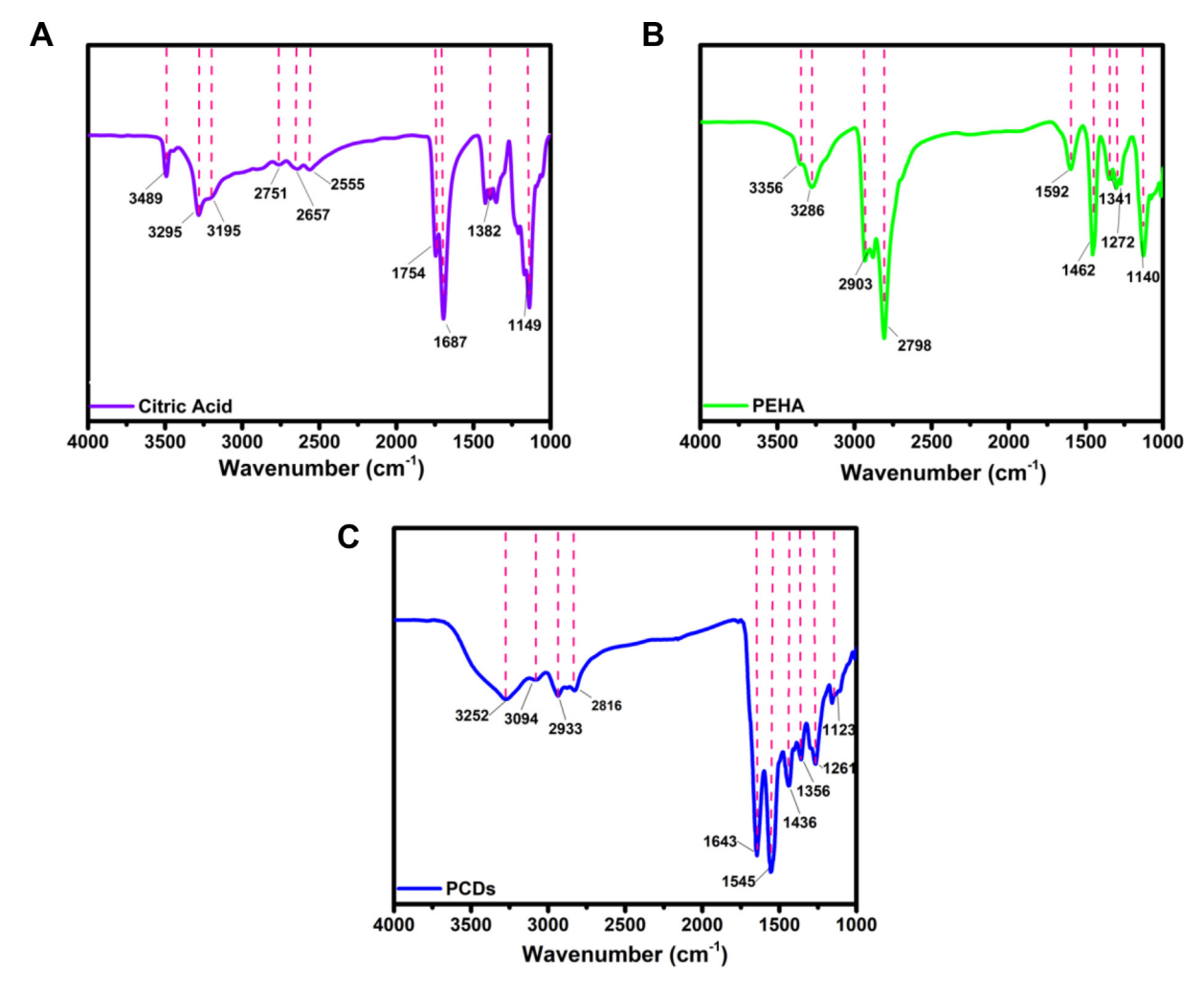


Fig. 2. FTIR spectra of (A) citric acid, (B) PEHA, and (C) PCDs.

sian distribution in the range of 0–10 nm. The average size of PCDs is around 2–6 nm based on the TEM measurements of more than 300 dots. Considering the mean particle sizes recorded by these two different microscopic techniques, PCDs are likely to possess a spherical shape and an average diameter of 2–6 nm.

3.2. DNA binding study

A plethora of compounds can bind with DNA via non-covalent interactions including electrostatic force, hydrogen bonding, van der Waals and hydrophobic interactions. Based on target positions

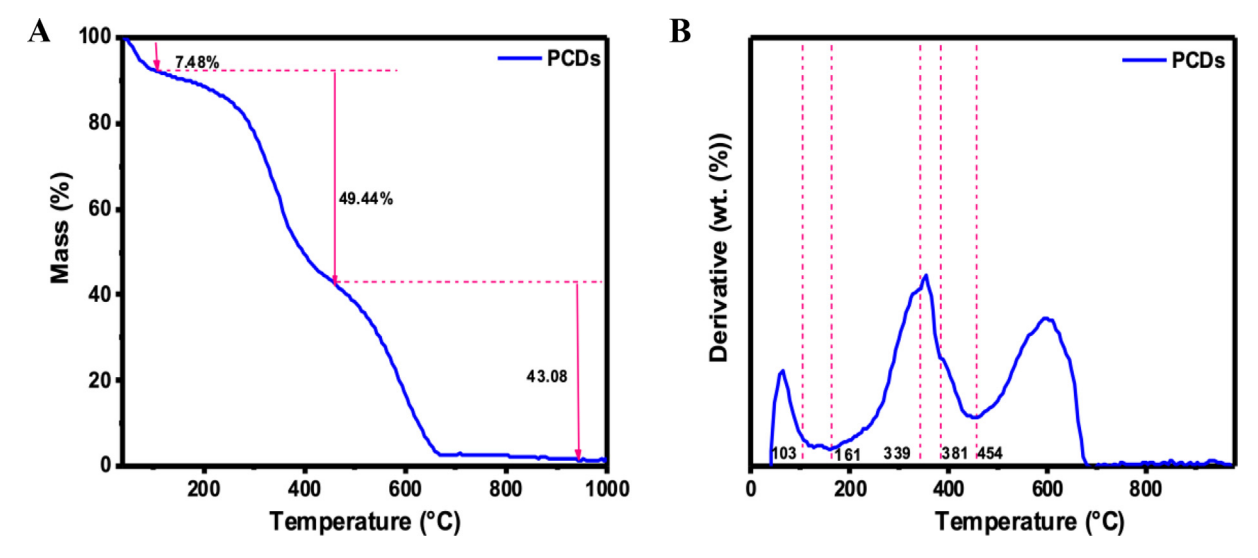


Fig. 3. (A) TGA and (B) DTG of PCDs.

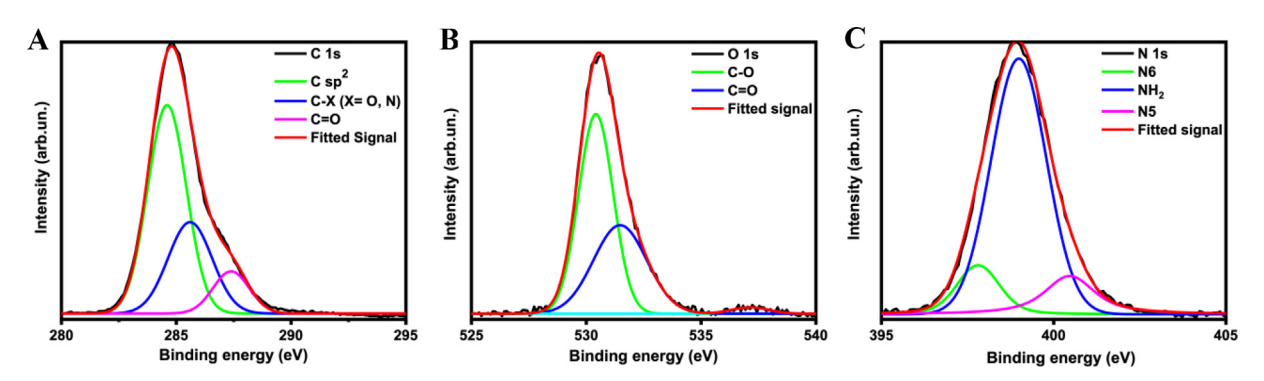


Fig. 4. XPS spectra of (A) C1s, (B) O1s and (C) N1s of PCDs.

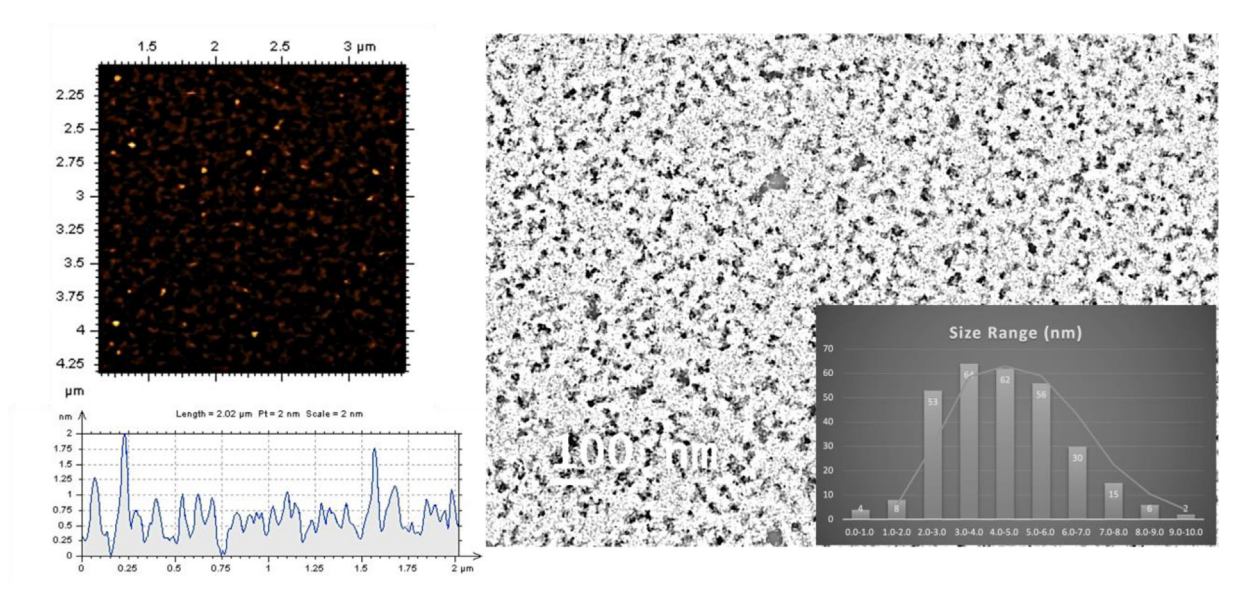


Fig. 5. (A) An AFM image with size distribution of PCDs; (B) A TEM image with size distribution histogram of PCDs. Scale bar is 100 nm.

in DNA, they can be categorized into intercalative, groove and electrostatic external bindings. Among them, intercalative binding relates to a process where molecules containing aromatic or heteroaromatic rings insert in between adjacent base pairs of

DNA by π – π stacking interactions without breaking up the hydrogen bonds between the DNA bases. Groove interactions involve the arc shaped, planar and unfused aromatic compounds that can be attracted to the minor/major groove of DNA and match the curva-

ture of the DNA double helix. External binding is related to interactions between compounds and DNA phosphate backbones via electrostatic interactions [43]. In this study, agarose gel electrophoresis and spectroscopic methods were applied to investigate the interaction and mechanism between PCDs and DNA.

3.2.1. Agarose gel retardation assay

The interaction between the as-synthesized PCDs and DNA was evaluated by agarose gel retardation at different mass ratios of PCDs to DNA ranging from 0:1 to 2:1. To analyze the impact of molecular weight of DNA on DNA-PCDs interactions, DNA with 317, 734, and 1688 bp were used. As displayed in Fig. 6, the migration bands of DNA-PCDs complexes formed at mass ratios equal or lower than 0.2:1 (PCDs: DNA) were kept the same as a DNA-free control, which suggests no interactions between PCDs and DNA at those mass ratios. As the ratio increased, the molecular weight of DNA significantly affected the migration. To be specific, DNA-PCDs complexes composed of 1688 bp DNA was completely retarded. As migration bands were highly dependent on the size of DNA-PCDs complexes, complete retardations demonstrate that many PCDs were attached to 1688 bp DNA. In comparison, the complexes from 734 bp DNA only slightly migrated, and there was no obvious difference from the control when the DNA bp number was 317, which suggests that the DNA of larger molecular weights achieved higher affinities to PCDs. It is reasonable that DNA with more bp can provide more binding sites. Overall, based on the electrophoresis results, the as-synthesized PCDs can interact with DNA. Owing to the positive charge and π system in the structure of PCDs, the interaction mechanism may be associated to electrostatic interaction, π - π stacking and hydrogen bonding.

3.2.2. UV/vis absorption studies

From Fig. 7, PCDs exhibit two absorption bands at about 240 and 350 nm. A bathochromic shift (red shift) of 8 nm and a hyperchromic effect (increase intensity of the absorption peak) of 17 % occurred to the peak at 240 nm at a mass ratio of 1:2. With the addition of calf thymus DNA, the intensity of transition band at 350 nm displayed a hyperchromic effect and increased by 57.4, 27.8, 8.1 and 2.1 % at mass ratios of DNA to PCDs at 1:2, 1:4, 1:6 and 1:8, respectively. The data above demonstrates that higher mass ratios of DNA to PCDs may lead to more prominent hyperchromic effects. In general, molecules binding with DNA through intercalation are usually accompanied by hypochromism and bathochromism due to stacking interactions between molecules and DNA, which can be further explained by the molecular orbital theory. In intercalative binding, the π^* orbital of molecules will couple with the π orbital of DNA. As electrons are partially filled in the coupled π^* orbital, transition possibilities reduce, resulting in hypochromism [44]. Thus, the hyperchromic effect of DNA-PCDs complexes in Fig. 7. suggests that the intercalative binding between PCDs and DNA can be excluded. Meanwhile, intercalative binding is normally characterized by a red shift by around or above 15 nm [45]. Thus, the red shift of 8 nm at 240 nm and slightly shift at 350 nm tend to support the hypothesis that PCDs bound with DNA through groove or electrostatic external binding.

3.2.3. Fluorescence emission studies

The fluorescence emission spectra of PCDs in the absence and presence of DNA were recorded and compared to further examine the DNA binding ability of PCDs. Considering the high sensitivity of fluorescence spectroscopy, the mass ratios of DNA to PCDs were set as 1:1, 1:2, 1:3, 1:4, 1:5, 1:6, 1:7 and 1:8. As shown in Fig. 8A, the fluorescence intensities of DNA-PCDs complexes were gradually enhanced with an increase in the mass ratio. The effect of DNA on fluorescence emission of PCDs is presented in Fig. 8B, which clearly demonstrates that DNA tremendously quenched the PL of

PCDs, proving a strong interaction between DNA and PCDs. The fluorescence intensity of DNA-PCDs complexes tended to remain constant when the concentration of PCDs was increased and higher than 87.5 μ g/L (or a mass ratio of 1:7), which is consistent with literature published previously [46]. The most prominent PL quenching (45.8 %) was observed to occur at the mass ratio of 1:8. Molecules binding with DNA via electrostatic force and groove binding would prefer radiationless deactivation and showed fluorescence quenching [43]. Since the PL quenching of PCDs in Fig. 8B was all higher than 30 % at different mass ratios, it is reasonable that PCDs bound with DNA by groove or external electrostatic interactions.

3.2.4. Circular dichroism studies

The circular dichroism spectra of DNA and DNA-PCD complexes at different mass ratios of DNA to PCDs were drawn in Fig. 9. The concentration of PCDs in Fig. 9B was 0.4 mg/mL, which was the highest concentration of PCDs used in DNA-PCDs complexation. It was found that PCDs alone did not show signals, suggesting that PCDs are achiral. Naked DNA displayed a negative band at 245 nm as a feature of right-handed DNA helical geometry and a positive band at 275 nm associated to base stacking of B form DNA (B-DNA) which is a right-handed DNA and is also the most common form of DNA. On the contrary, the left-handed DNA is called Z form DNA (Z-DNA). With addition of PCDs, the band at 275 nm decreased and showed a negative band at 285 nm, while the band at 245 nm switched to a positive one. Hence, circular dichroism spectral analyses pointed out that PCDs can facilitate the B-Z DNA transition. In terms of DNA conformation, a factor to trigger the B-Z transition is shielding of the electrostatic repulsion from the phosphate groups of DNA. In physiological environment, the electrostatic repulsion from the phosphate groups will push the conformation of DNA to B form. In the presence of cations, repulsions will be attenuated, and DNA prefers Z form whose adjacent phosphate oxygens were 1 Å distant and closer than that in B-DNA [47-49]. Considering that PCDs in this study have plenty of amine groups and positive charges, thus the electrostatic external binding between amine groups of PCDs and phosphate groups of DNA might be the main reason for the conformation transition. Furthermore, compared with 1:2, 1:4 and 1:6 with 1:8, it was evident that the typical bands of Z-DNA at a mass ratio of 1:8 were dramatically enhanced. In addition to the phosphate distance, the absence of major grooves in Z-DNA is another structural difference between Z-DNA and B-DNA. Bhanjadeo and Subudhi early reported that minor groove binders such as DAPI and Hoechst 3342 could increase the absorbance of DNA [50]. Since the induced Z-DNA after treatment of PCDs did not have major grooves, the significant change from 1:6 to 1:8 is interpreted by minor groove binding of PCDs to Z-DNA. This groove binding could be explained by the shape of PCDs and the intrinsic structure of DNA. From AFM and TEM, it has been proved that PCDs are elliptical shape. These elliptical PCDs might provide partial arc shaped structure which could attach to the DNA and match the curvature of DNA double helix, forming the groove binding. Therefore, the circular dichroism spectra suggest that the DNA binding mechanisms of PCDs mainly focus on electrostatic and groove modes (especially minor groove binding).

3.3. In vitro cytotoxicity study

In this study, the cytotoxicity of PCDs was investigated since except for a high transfection efficiency, a low cytotoxicity is another utmost important requirement PCDs need to meet. The *in vitro* cytotoxicity of PCDs was measured using MTT assay with HEK 293 cells. In addition, the comparison between PCDs and PEI (10 kDa) in terms of cytotoxicity is included. In Fig. 10, PEI shows

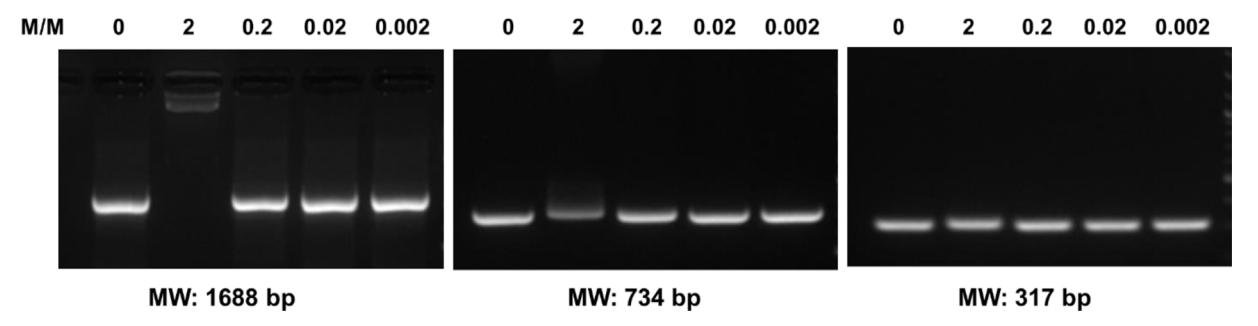


Fig. 6. Agarose gel electrophoresis of DNA-PCDs complexes at different mass ratios of PCDs to DNA (0.002:1, 0.02:1, 0.2:1, 2:1) for various base pairs (bp).

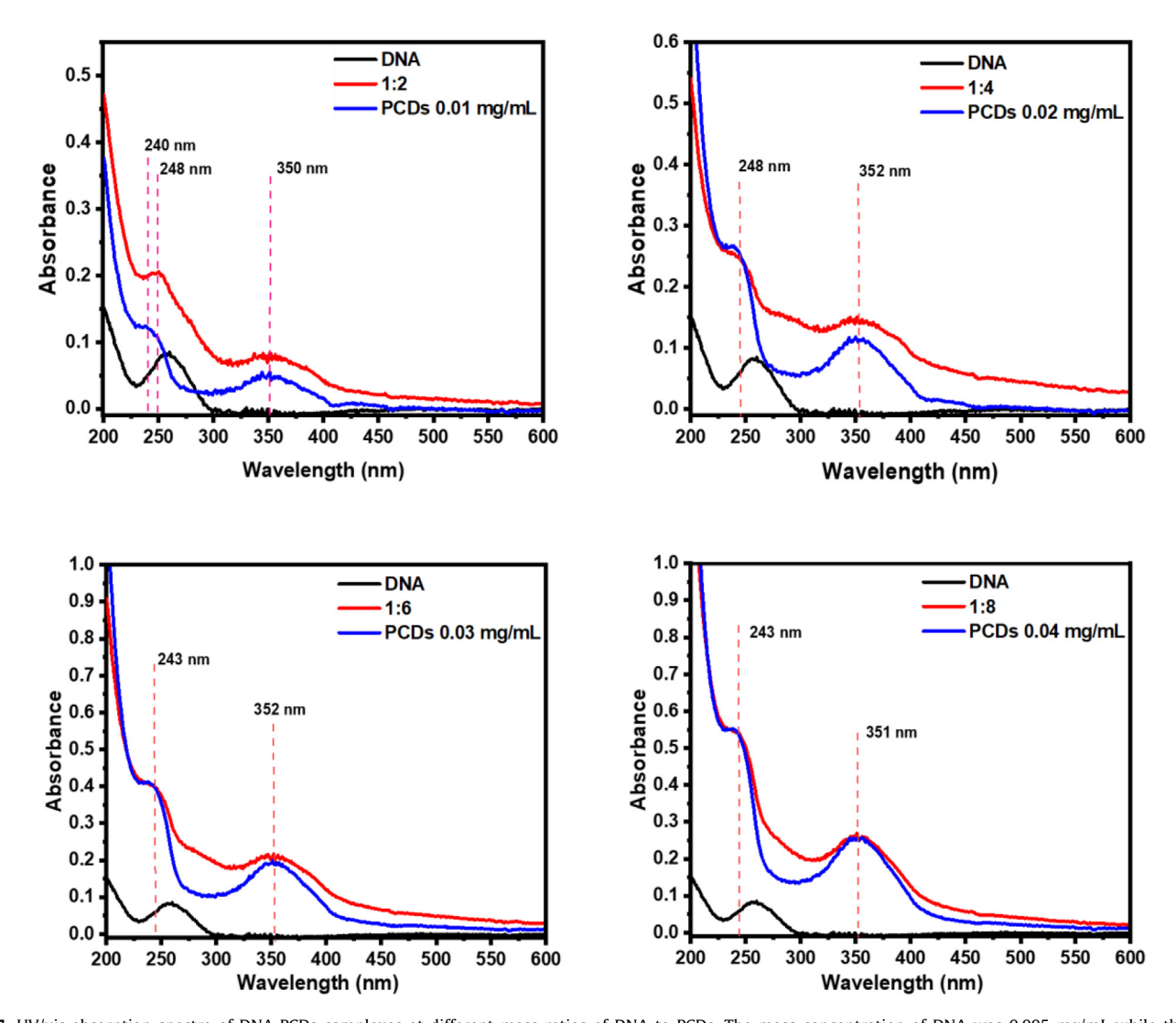


Fig. 7. UV/vis absorption spectra of DNA-PCDs complexes at different mass ratios of DNA to PCDs. The mass concentration of DNA was 0.005 mg/mL while the mass concentration of PCDs ranged from 0.01 to 0.04 mg/mL.

a high toxicity, even at a low concentration of 3.91 $\mu g/mL$. In comparison, when the concentration of PCDs was up to 62.5 $\mu g/mL$, the cell viability was still higher than 70 % after 72 h incubation, which was similar to that of the PEHA treatment group. Furthermore, compared with PEHA, PCDs showed negligible cytotoxicity at low concentrations such as 7.81 $\mu g/mL$. Thus, the as-prepared PCDs are biocompatible and safety enough to be applied as nanocarriers in the biomedical field.

3.4. In vitro transfection

The transfection efficiency of PCDs was assessed by delivering a plasmid DNA (pDNA) that expresses green fluorescence protein (GFP) or red fluorescence protein (mCh) into HEK 293 cells. As displayed by Fig. 11B, neither PCDs nor pDNA-GFP (GFP plasmid) group were observed fluorescence signals in cells, suggesting that the fluorescence of PCDs would not interfere with the results in

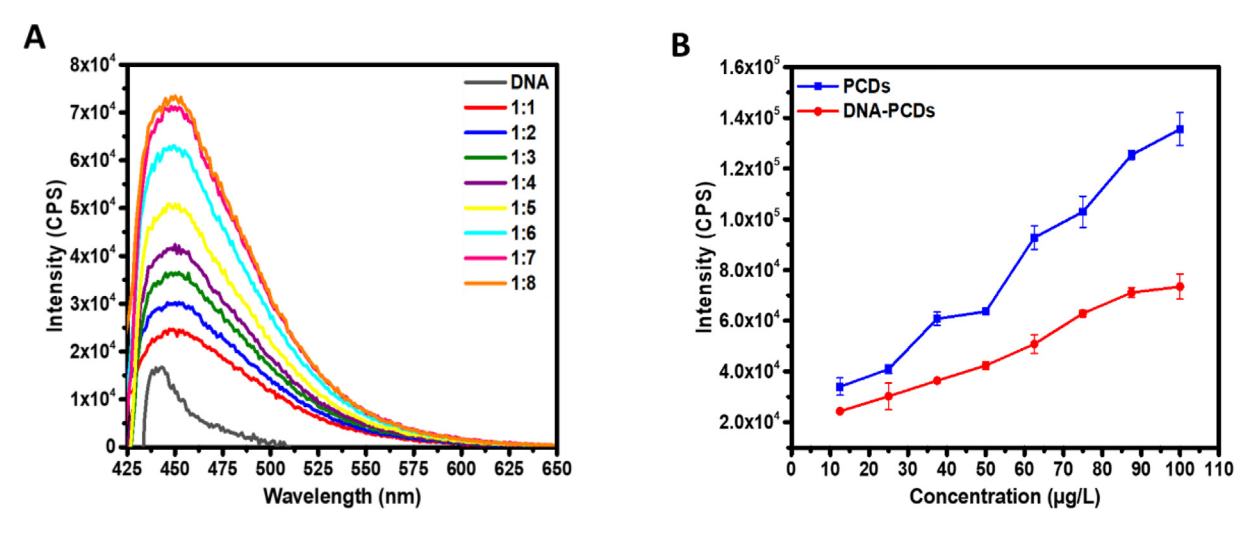


Fig. 8. (A) The fluorescence spectra of DNA-PCDs complexes at different mass ratios excited at 370 nm; (B) Comparison of emission intensities at 450 nm between the PCDs and DNA-PCDs complexes. The concentration of DNA was 12.5 µg/L and the concentrations of PCDs ranged from 12.5 to 100 µg/L. Data are presented by mean ± SEM.

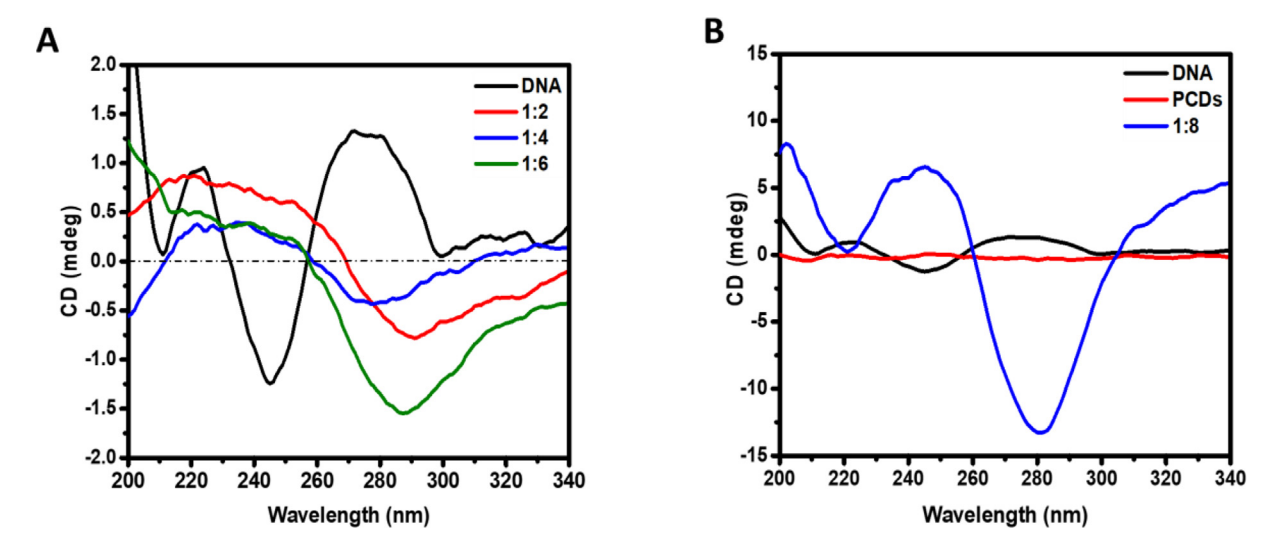


Fig. 9. Circular dichroism spectra of DNA, PCDs and DNA-PCDs complexes. The labels of 1:2, 1:4, 1:6 and 1:8 represent the mass ratio of DNA to PCDs in DNA-PCDs complexes formation. The mass concentration of DNA was 0.05 mg/mL; The mass concentrations of PCDs ranged from 0.1 to 0.4 mg/mL.

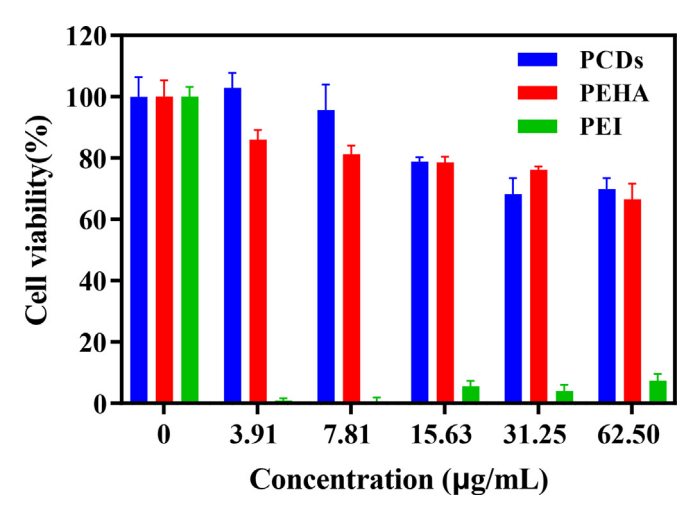


Fig. 10. Cytotoxicity measurements of PCDs, PEHA and PEI at different concentrations that were applied to incubate HEK 293 cells for 72 h. The cell viability of control was taken as 100 %. Data are exhibited as the mean ± SEM.

the GFP channel and GFP could not be expressed in pDNA-GFP group without any vectors. It can be explained by the fact that nuclei acids are poorly permeable through the cell membrane [51]. However, after pDNA-GFP were mixed with PCDs and incubated for 24 h, green fluorescence signals were clearly detected by a fluorescence microscope. From Fig. 11A, when the mass ratio of PCDs to pDNA-GFP was increased from 1:20 to 1:50, the transfection efficiency was improved. Meanwhile, the mCherry expressed from pDNA-mCh further demonstrated the possibility of utilizing PCDs as a universal transfection vector.

To quantify the GFP protein expression in HEK 293 cells, Western blot was performed. As shown in Fig. 12A, the GFP protein signal was not observed in both pDNA-GFP-and PCDs-treated cells. It is consistent with the results shown by fluorescence microscopy images in Fig. 11B. The complex composed of pDNA-GFP and PCDs at a 1:50 mass ratio displays the highest GFP/ β -actin ratio (Fig. 12B). The transfection capacity of PCDs was not improved by either increasing or decreasing the mass of PCDs and 1:50 (PCDs: pDNA) was the best mass ratio for plasmid transfection.

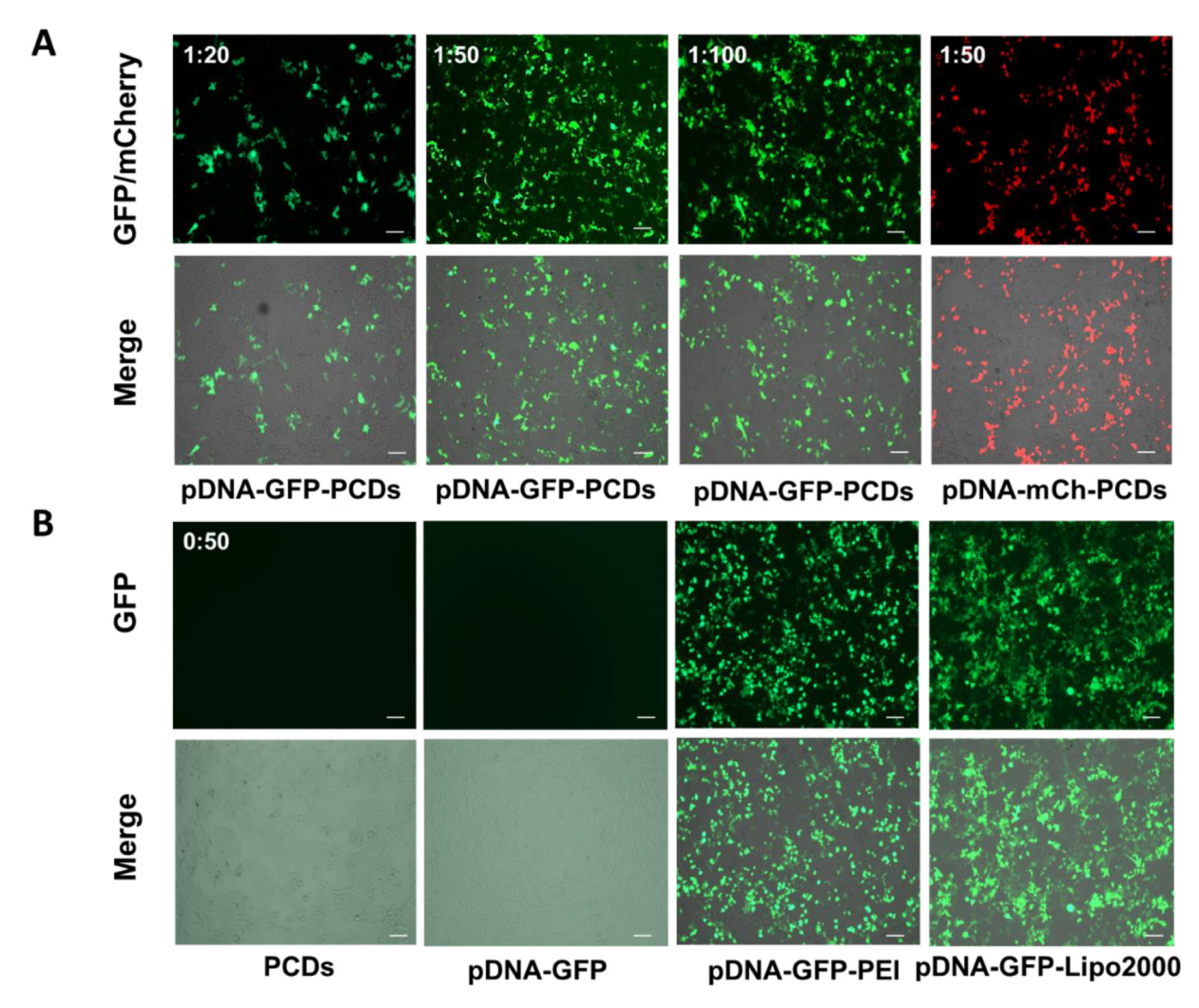


Fig. 11. (A) Transfection of pDNA-PCDs at different mass ratios of pDNA to PCDs in HEK 293 cells. (B) Negative controls that cells were only treated with PCDs or pDNA and positive controls that cells were treated with PEI or lipo2000 linked to pDNA. Merge: GFP or mCh channel was merged with that of bright field.

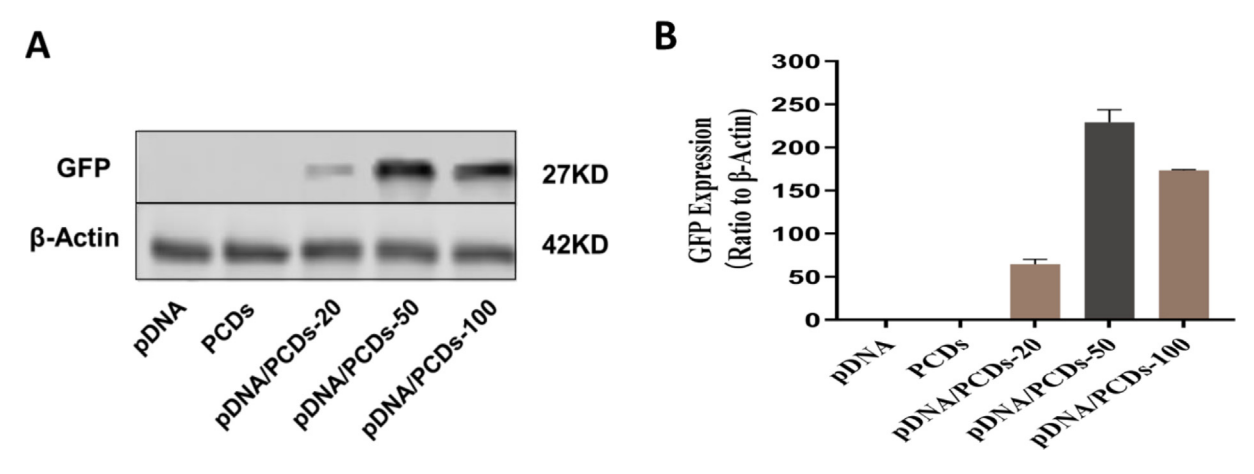


Fig. 12. (A) GFP expression mediated by different vectors in HEK 293 cells;(B) Quantification of GFP expression (n = 3). Data are displayed as the mean ± SEM.

3.5. The blood-brain barrier penetration

Zebrafish has a similar central nervous system (CNS) physiology to human, which contains all major components including transmitters, hormones, and receptors [52]. Compared to mice, zebrafish can reproduce more offspring to provide enough animal models for any research. Also, zebrafish offspring are more affordable and don't require much space to accommodate. Moreover, the embryos and larvae of zebrafish are transparent, which benefits the observation [53]. In order to determine whether PCDs possess

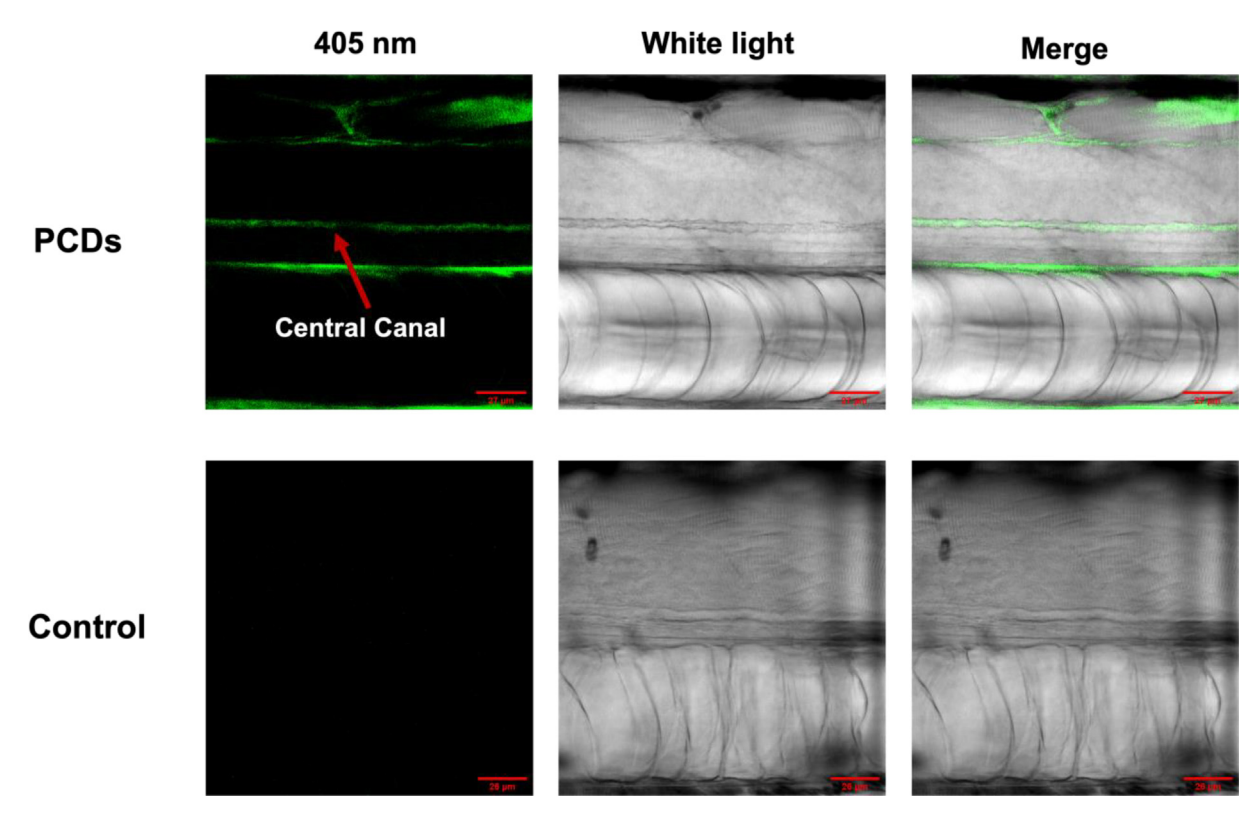


Fig. 13. Confocal images of zebrafish larvae injected with PCD aqueous solution (50 mg/ml) in contrast to the control group. The red arrow indicates the central canal of spinal cord of zebrafish. Each picture was reproduced with at least six larvae. (For interpretation of the references to colour in this figure legend, the reader is referred to the web version of this article.)

the ability to cross the BBB, zebrafish was employed as *in vivo* model. In detail, a high mass concentration (50 mg/mL) of PCDs aqueous solution was prepared and intravascularly injected into the heart of 5 dpf wild-type zebrafish larvae. Under the excitation wavelength of 405 nm, a blue PL in the central canal of spinal cord shown in Fig. 13 indicates the arrival of PCDs in the CNS. In contrast to the control group, it demonstrates that the PCDs could cross the BBB. From this point of view, PCDs, also, are potential drug delivery nanocarriers targeting brain disorders and diseases.

4. Conclusion

On the basis of the previously reported PEHA-derived CDs, the PCDs synthesized in this work were the first reported CDs using only citric acid and PEHA as precursors. A series of characterizations including UV/vis absorption, fluorescence emission, FTIR, TGA, DTG, XPS, AFM, TEM, circular dichroism spectrometry and zeta potential measurements were applied to investigate the optical, and electrical properties, structure and morphology of PCDs. PCDs were observed with spherical morphology, excitationdependent PL, and positive surface charges. Agarose gel electrophoresis demonstrated that PCDs could bind to DNA. Based on the analysis of UV/vis absorption, fluorescence emission and circular dichroism spectroscopic results, the binding mechanisms were mainly centered on electrostatic interactions between the positively-charged amine groups of PCDs and negatively-charged phosphate groups of DNA, and groove interactions especially minor groove adsorption. In addition, both in vitro cytotoxicity and transfection studies demonstrated that PCDs not only have a high transfection capacity, but also a tremendously lower cytotoxicity compared with PEI. Interestingly, later, confocal images suggested that PCDs could cross the BBB and enter the CNS of zebrafish. In

conclusion, the as-prepared PCDs are biocompatible and able to penetrate the BBB and cell membrane, and bind with DNA while carrying plasmid for transfection. Further study about the relationship between the structure of PCDs and their DNA binding affinity is under way. In addition, using PCDs for bioimaging and as gene vectors to transfect cells and deliver genes/drugs to treat brain diseases are also promising direction.

CRediT authorship contribution statement

Wei Zhang: Conceptualization, Methodology, Validation, Formal analysis. Investigation, Data curation, Writing – original draft. Writing - review & editing, Project administration. Jiuyan Chen: Conceptualization, Methodology, Validation, Formal analysis, Investigation, Writing - original draft, Writing - review & editing, Project administration. Jun Gu: Methodology, Validation, Formal analysis, Investigation. Mattia Bartoli: Methodology, Validation, Formal analysis, Investigation, Writing - original draft. Justin B. Domena: Methodology, Validation, Investigation. Yiqun Zhou: Formal analysis, Investigation, Writing - review & editing. Braulio C.L.B. Ferreira: Methodology, Validation, Investigation. Emel Kirbas Cilingir: Methodology, Validation, Investigation. Caitlin M. McGee: . Rachel Sampson: . Chiara Arduino: Investigation. Alberto Tagliaferro: Formal analysis, Investigation. Roger M. Leblanc: Conceptualization, Resources, Supervision, Funding acquisition, Visualization, Methodology, Project administration, Writing - review & editing.

Data availability

The data that has been used is confidential.

Declaration of Competing Interest

The authors declare that they have no known competing financial interests or personal relationships that could have appeared to influence the work reported in this paper.

Acknowledgements

Professor Roger M. Leblanc thanks the support from the National Science Foundation (United States) under the grant 2041413 and the National Institute of Health (United States) under the grant SUB00002778. The authors gratefully acknowledge the great support from the University of Miami, USA.

Appendix A. Supplementary material

Supplementary data to this article can be found online at https://doi.org/10.1016/j.jcis.2023.02.046.

References

- [1] T.A. Ajith, Strategies used in the clinical trials of gene therapy for cancer, J. Exp. Ther. Oncol. 11 (2015) 33–39.
- [2] M. Haider, Z. Megeed, H. Ghandehari, Genetically engineered polymers: Status and prospects for controlled release, J. Control. Release 95 (2004) 1–26.
- [3] E. Mastrobattista, M.A. van der Aa, W.E. Hennink, D.J. Crommelin, Artificial viruses: A nanotechnological approach to gene delivery, Nat. Rev. Drug Discov. 5 (2006) 115–121.
- [4] B.W. Hwang, S.J. Kim, K.M. Park, H. Kim, J. Yeom, J.-A. Yang, H. Jeong, H. Jung, K. Kim, Y.C. Sung, S.K. Hahn, Genetically engineered mesenchymal stem cell therapy using self-assembling supramolecular hydrogels, J. Control. Release 220 (2015) 119–129.
- [5] M. Croyle, X. Cheng, J. Wilson, Development of formulations that enhance physical stability of viral vectors for gene therapy, Gene Ther. 8 (2001) 1281– 1290
- [6] W. Chen, S. Yao, J. Wan, Y. Tian, L. Huang, S. Wang, F. Akter, Y. Wu, Y. Yao, X. Zhang, BBB-crossing adeno-associated virus vector: An excellent gene delivery tool for CNS disease treatment, J. Control. Release 333 (2021) 129–138.
- [7] M. Foldvari, D.W. Chen, N. Nafissi, D. Calderon, L. Narsineni, A. Rafiee, Non-viral gene therapy: Gains and challenges of non-invasive administration methods, J. Control. Release 240 (2016) 165–190.
- [8] H. Zu, D. Gao, Non-viral vectors in gene therapy: Recent development, challenges, and prospects, AAPS J. 23 (2021) 1–12.
- [9] G.R. Ediriweera, L. Chen, J.J. Yerbury, K.J. Thurecht, K.L. Vine, Non-viral vector-mediated gene therapy for ALS: Challenges and future perspectives, Mol. Pharm. 18 (2021) 2142–2160.
- [10] Y.K. Sung, S.W. Kim, Recent advances in the development of gene delivery systems, Biomater. Res. 23 (2019) 1–7.
- [11] S. Kuriyama, A. Mitoro, H. Tsujinoue, T. Nakatani, H. Yoshiji, T. Tsujimoto, M. Yamazaki, H. Fukui, Particle-mediated gene transfer into murine livers using a newly developed gene gun, Gene Ther. 7 (2000) 1132–1136.
- [12] Y. Sakakima, S. Hayashi, Y. Yagi, A. Hayakawa, K. Tachibana, A. Nakao, Gene therapy for hepatocellular carcinoma using sonoporation enhanced by contrast agents, Cancer Gene Ther. 12 (2005) 884–889.
- [13] L. Paterson, B. Agate, M. Comrie, R. Ferguson, T.K. Lake, J.E. Morris, A.E. Carruthers, C.T.A. Brown, W. Sibbett, P.E. Bryant, F. Gunn-Moore, A.C. Riches, K. Dholakia, Photoporation and cell transfection using a violet diode laser, Opt. Express 13 (2005) 595–600.
- [14] F. Scherer, M. Anton, U. Schillinger, J. Henke, C. Bergemann, A. Krüger, B. Gänsbacher, C. Plank, Magnetofection: Enhancing and targeting gene delivery by magnetic force in vitro and in vivo, Gene Ther. 9 (2002) 102–109.
- [15] M.P. Stewart, R. Langer, K.F. Jensen, Intracellular delivery by membrane disruption: Mechanisms, strategies, and concepts, Chem. Rev. 118 (2018) 7409–7531.
- [16] M.A. Mintzer, E.E. Simanek, Nonviral vectors for gene delivery, Chem. Rev. 109 (2009) 259–302.
- [17] H. Aihara, J.-I. Miyazaki, Gene transfer into muscle by electroporation in vivo, Nat. Biotechnol. 16 (1998) 867–870.
- [18] R. Kanwar, M. Gradzielski, S. Prevost, G. Kaur, D. Clemens, M.-S. Appavou, S.K. Mehta, Effect of lipid chain length on nanostructured lipid carriers: Comprehensive structural evaluation by scattering techniques, J. Colloid Interface Sci. 534 (2019) 95–104.
- [19] M.A. Khan, V.M. Wu, S. Ghosh, V. Uskoković, Gene delivery using calcium phosphate nanoparticles: Optimization of the transfection process and the effects of citrate and poly(l-lysine) as additives, J. Colloid Interface Sci. 471 (2016) 48–58.
- [20] M. Massaro, G. Barone, G. Biddeci, G. Cavallaro, F. Di Blasi, G. Lazzara, G. Nicotra, C. Spinella, G. Spinelli, S. Riela, Halloysite nanotubes-carbon dots hybrids multifunctional nanocarrier with positive cell target ability as a

- potential non-viral vector for oral gene therapy, J. Colloid Interface Sci. 552 (2019) 236–246.
- [21] X. Yang, Y. Wang, X. Shen, C. Su, J. Yang, M. Piao, F. Jia, G. Gao, L. Zhang, Q. Lin, One-step synthesis of photoluminescent carbon dots with excitationindependent emission for selective bioimaging and gene delivery, J. Colloid Interface Sci. 492 (2017) 1–7.
- [22] D. Putnam, Polymers for gene delivery across length scales, Nat. Mater. 5 (2006) 439-451.
- [23] D.W. Pack, A.S. Hoffman, S. Pun, P.S. Stayton, Design and development of polymers for gene delivery, Nat. Rev. Drug Discov. 4 (2005) 581–593.
- [24] S.C. Semple, A. Akinc, J. Chen, A.P. Sandhu, B.L. Mui, C.K. Cho, D.W.Y. Sah, D. Stebbing, E.J. Crosley, E. Yaworski, I.M. Hafez, J.R. Dorkin, J. Qin, K. Lam, K.G. Rajeev, K.F. Wong, L.B. Jeffs, L. Nechev, M.L. Eisenhardt, M. Jayaraman, M. Kazem, M.A. Maier, M. Srinivasulu, M.J. Weinstein, Q. Chen, R. Alvarez, S.A. Barros, S.De, S.K. Klimuk, T. Borland, V. Kosovrasti, W.L. Cantley, Y.K. Tam, M. Manoharan, M.A. Ciufolini, M.A. Tracy, A. de Fougerolles, I. MacLachlan, P.R. Cullis, T.D. Madden, M.J. Hope, Rational design of cationic lipids for siRNA delivery, Nat. Biotechnol. 28 (2010) 172–176.
- [25] V. Mishra, A. Patil, S. Thakur, P. Kesharwani, Carbon dots: Emerging theranostic nanoarchitectures, Drug Discov. Today 23 (2018) 1219–1232.
- [26] X. Cao, J. Wang, W. Deng, J. Chen, Y. Wang, J. Zhou, P. Du, W. Xu, Q. Wang, Q. Wang, Q. Yu, M. Spector, J. Yu, X. Xu, Photoluminescent cationic carbon dots as efficient non-viral delivery of plasmid SOX9 and chondrogenesis of fibroblasts, Sci. Rep. 8 (2018) 1–11.
- [27] M. Algarra, M. Pérez-Martín, M. Cifuentes-Rueda, J. Jiménez-Jiménez, J.C.G. Esteves da Silva, T.J. Bandosz, E. Rodríguez-Castellón, J.T. López Navarrete, J. Casado, Carbon dots obtained using hydrothermal treatment of formaldehyde, Cell imaging in vitro, Nanoscale 6 (2014) 9071–9077.
- [28] S.-L. Hu, K.-Y. Niu, J. Sun, J. Yang, N.-Q. Zhao, X.-W. Du, One-step synthesis of fluorescent carbon nanoparticles by laser irradiation, J. Mater. Chem. 19 (2009) 484–488.
- [29] B. Wang, J. Huang, M. Zhang, Y. Wang, H. Wang, Y. Ma, X. Zhao, X. Wang, C. Liu, H. Huang, Y. Liu, F. Lu, H. Yu, M. Shao, Z. Kang, Carbon dots enable efficient delivery of functional DNA in plants, ACS Applied Bio Materials 3 (2020) 8857– 8864
- [30] S. Kumari, S. Rajit Prasad, D. Mandal, P. Das, Carbon dot-DNA-protoporphyrin hybrid hydrogel for sustained photoinduced antimicrobial activity, J. Colloid Interface Sci. 553 (2019) 228–238.
- [31] V. Lisa John, F. Joy, A. Jose Kollannoor, K. Joseph, Y. Nair, V. T. P, Amine functionalized carbon quantum dots from paper precursors for selective binding and fluorescent labelling applications, Journal of Colloid and Interface Science, 617 (2022), 730–744.
- [32] L. Hu, Y. Sun, S. Li, X. Wang, K. Hu, L. Wang, X.-J. Liang, Y. Wu, Multifunctional carbon dots with high quantum yield for imaging and gene delivery, Carbon 67 (2014) 508–513.
- [33] L.-J. Yue, Y.-Y. Wei, J.-B. Fan, L. Chen, Q. Li, J.-L. Du, S.-P. Yu, Y.-Z. Yang, Research progress in the use of cationic carbon dots for the integration of cancer diagnosis with gene treatment, New Carbon Mater. 36 (2021) 373–389.
- [34] W. Meng, A. Rey-Rico, M. Claudel, G. Schmitt, S. Speicher-Mentges, F. Pons, L. Lebeau, J.K. Venkatesan, M. Cucchiarini, rAAV-mediated overexpression of SOX9 and TGF-β via carbon dot-guided vector delivery enhances the biological activities in human bone marrow-derived mesenchymal stromal cells, Nanomaterials 10 (2020) 1-16.
- [35] P.Y. Liyanage, R.M. Graham, R.R. Pandey, C.C. Chusuei, K.J. Mintz, Y. Zhou, J.K. Harper, W. Wu, A.H. Wikramanayake, S. Vanni, Carbon nitride dots: A selective bioimaging nanomaterial, Bioconjug. Chem. 30 (2018) 111–123.
- [36] W. Zhang, N. Kandel, Y. Zhou, N. Smith, B.C. Ferreira, M. Perez, M.L. Claure, K.J. Mintz, C. Wang, R.M. Leblanc, Drug delivery of memantine with carbon dots for Alzheimer's disease: Blood-brain barrier penetration and inhibition of tau aggregation, J. Colloid Interface Sci. 617 (2022) 20–31.
 [37] E. Kirbas Cilingir, E.S. Seven, Y. Zhou, B.M. Walters, K.J. Mintz, R.R. Pandey, A.H.
- [37] E. Kirbas Cilingir, E.S. Seven, Y. Zhou, B.M. Walters, K.J. Mintz, R.R. Pandey, A.H. Wikramanayake, C.C. Chusuei, S. Vanni, R.M. Graham, R.M. Leblanc, Metformin derived carbon dots: Highly biocompatible fluorescent nanomaterials as mitochondrial targeting and blood-brain barrier penetrating biomarkers, J. Colloid Interface Sci. 592 (2021) 485–497.
- [38] N.J. Venkatesha, S. Ramesh, Citric acid-assisted synthesis of nanoparticle copper catalyst supported on an oxide system for the reduction of furfural to furfuryl alcohol in the vapor phase, Ind. Eng. Chem. Res. 57 (2018) 1506–1515.
- [39] M. Mecozzi, E. Sturchio, Computer assisted examination of infrared and near infrared spectra to assess structural and molecular changes in biological samples exposed to pollutants: a case of study, Journal of, Imaging 3 (2017) 1– 13
- [40] Y. Zhou, N. Kandel, M. Bartoli, L.F. Serafim, A.E. ElMetwally, S.M. Falkenberg, X. E. Paredes, C.J. Nelson, N. Smith, E. Padovano, W. Zhang, K.J. Mintz, B. Ferreira, E.K. Cilingir, J. Chen, S.K. Shah, R. Prabhakar, A. Tagliaferro, C. Wang, R.M. Leblanc, Structure-activity relationship of carbon nitride dots in inhibiting tau aggregation, Carbon N Y 193 (2022) 1–16.
- [41] Y. Zhou, A. Desserre, S.K. Sharma, S. Li, M.H. Marksberry, C.C. Chusuei, P.L. Blackwelder, R.M. Leblanc, Gel-like carbon dots: Characterization and their potential applications, ChemPhysChem 18 (2017) 890–897.
- [42] H. Casellas, D. de Caro, L. Valade, J. Fraxedas, Thin films of hydroxy-TEMPOsubstituted TTF and of its charge-transfer complex with TCNQ, New J. Chem. 26 (2002) 915–919.
- [43] M.M. Aleksic, V. Kapetanovic, An overview of the optical and electrochemical methods for detection of DNA - drug interactions, Acta Chim Slov 61 (2014) 555–573.

- [44] M. Sirajuddin, S. Ali, N.A. Shah, M.R. Khan, M.N. Tahir, Synthesis, characterization, biological screenings and interaction with calf thymus DNA of a novel azomethine 3-((3,5-dimethylphenylimino)methyl)benzene-1,2-diol, Spectrochim. Acta A Mol. Biomol. Spectrosc. 94 (2012) 134–142.
- [45] S.S. Kalanur, U. Katrahalli, J. Seetharamappa, Electrochemical studies and spectroscopic investigations on the interaction of an anticancer drug with DNA and their analytical applications, J. Electroanal. Chem. 636 (2009) 93–100.
- [46] C.-Y. Liang, W. Xia, C.-Z. Yang, Y.-C. Liu, A.-M. Bai, Y.-J. Hu, Exploring the binding of carbon dots to calf thymus DNA: from green synthesis to fluorescent molecular probe, Carbon 130 (2018) 257–266.
- [47] T. Qin, K. Liu, D. Song, C. Yang, H. Zhao, H. Su, Binding interactions of zinc cationic porphyrin with duplex DNA: from B-DNA to Z-DNA, Int. J. Mol. Sci. 19 (2018) 1–12.
- [48] A.K. Nayak, A. Mishra, B.S. Jena, B.K. Mishra, U. Subudhi, Lanthanum induced B-to-Z transition in self-assembled Y-shaped branched DNA structure, Scientific Report 6 (2016) 1–11.

- [49] L. Feng, A. Zhao, J. Ren, X. Qu, Lighting up left-handed Z-DNA: Photoluminescent carbon dots induce DNA B to Z transition and perform DNA logic operations, Nucleic Acids Res. 41 (2013) 7987–7996.
- [50] M.M. Bhanjadeo, U. Subudhi, Praseodymium promotes B-Z transition in self-assembled DNA nanostructures, RSC Adv. 9 (2019) 4616–4620.
- [51] B.B. Mendes, J. Conniot, A. Avital, D. Yao, X. Jiang, X. Zhou, N. Sharf-Pauker, Y. Xiao, O. Adir, H. Liang, J. Shi, A. Schroeder, J. Conde, Nanodelivery of nucleic acids, Nat. Rev. Methods Primers 2 (2022) 1–21.
- [52] W. Zhang, G. Sigdel, K.J. Mintz, E.S. Seven, Y. Zhou, C. Wang, R.M. Leblanc, Carbon Dots: A future blood-Brain barrier penetrating nanomedicine and drug nanocarrier, Int. J. Nanomed. 16 (2021) 5003–5016.
- [53] Y. Zhou, P.Y. Liyanage, D. Devadoss, L.R. Rios Guevara, L. Cheng, R.M. Graham, H.S. Chand, A.O. Al-Youbi, A.S. Bashammakh, M.S. El-Shahawi, R.M. Leblanc, Nontoxic amphiphilic carbon dots as promising drug nanocarriers across the blood-brain barrier and inhibitors of β-amyloid, Nanoscale 11 (2019) 22387– 22397.